Highlights for:

Unsteady experimental and numerical analysis of a two-phase closed thermosyphon at different filling ratios

- ✓ Thermal behavior of two-phase closed thermosyphon under normal and operating limitation is experimentally and numerically investigated.
- ✓ Axial temperature distribution of thermosyphon at different filling ratio is evaluated.
- ✓ Dryout, local dryout and geyser boiling limitation of the thermosyphon is examined in transient operation.
- ✓ The transient numerical model is well validated at normal operation, however, a discrepancy is observed in comparison of experimental data at optimum filling ratio.

Corresponding Author:

Davoud Jafari

Department of Energy, Systems, Territory and Constructions Engineering (DESTEC), University of Pisa, Largo Lucio Lazzarino, 2, 56126 PISA, Italy

Phone: +393472817717

Email: d.jafari@studenti.unipi.it, j.davoud@yahoo.com

Unsteady experimental and numerical analysis of a two-phase closed thermosyphon at different filling ratios

Davoud Jafari, Sauro Filippeschi, Alessandro Franco, Paolo Di Marco

Department of Energy, Systems, Territory and Constructions Engineering (DESTEC),

University of Pisa, Italy

Abstract

This paper deals with the experimental analysis and numerical simulation of a two-phase closed thermosyphon (TPCT) in the aim to predict its transient performances. A concern in the design and operation of TPCT is evaluating working fluid loading charge to maximize performance while avoiding dryout in the evaporator section and geyser boiling phenomena. The model includes the heat transfer through the wall, vapor core, liquid pool and the falling condensate film. The complete two-dimensional conservation equations for mass, momentum, and energy are solved using a finite volume scheme for the vapor flow and pipe wall. The liquid film is modeled by using one dimensional quasi-steady Nusselt type solution. An experimental facility has been also designed and operated to determine the operating condition and measure the maximum heat transport rate and the overall thermal resistance of the TPCT. The total length and diameter of pipe are 500 mm and 35 mm, respectively. The experiments have been performed in the heat transfer range of 30–700 W and filling ratios of 16, 35 and 135%. The numerical predictions for the maximum heat transport rate due to transient local dryout are shown to be in close agreement with the experimental results under normal operation. However, for obtained liquid film dryout a discrepancy is observed. The geyser boiling is also evaluated under certain operating condition.

Keywords: two-phase closed thermosyphon, operating limitation, numerical simulation, experimental analysis

---

1. INTRODUCTION

Heat pipes have emerged as the most appropriate technology and cost effective thermal control solution due to their excellent heat transfer capabilities [1, 2]. A special heat pipe where the condensed liquid moves to the condenser by gravity is two phase closed thermosyphon (TPCT), without capillary structure. TPCT can be used in much wider thermal and temperature ranges than a wicked heat pipe, since it does not have the large flow resistance or low boiling limit inside the wick, as the condensate liquid in the TPCT is returned to the heated side of the system under the effect of gravity, instead of capillary forces in wicked HPs. Thermosyphon can operate even against gravity with good performance with respect to the classical capillary loops [3]. However, TPCTs have major limits on the maximum amount of thermal energy that can be transferred due mainly to dryout, flooding and entrainment limits [4].

Thermosyphon is a highly performing device if applied to ground thermal engineering applications and in particular for solar energy systems. TPCTs could also find application in chemical and petroleum industry, electronic cooling, telecommunication devices, energy storage systems, railway transportation systems, thermoelectric power generators, and defrosting applications in heat pumps [5-13].

Even their large use, their design is basically only few inaccurate correlations that have been mostly developed for two-phase thermosyphon in vertical position. The use of TPCTs for different heat transfer applications has led to develop several mathematical modeling and predictive tools. In the effort to meet this demand, several papers has been presented dealing with tools ranging from the simple lumped capacity models [14-16] up to complex transient multi-dimensional simulation. The most complex modeling approaches are based on the physical equations which describe the heat and mass flow rate in all the thermosyphon sections: evaporator, adiabatic and condenser zones. In these models, vapor and liquid inside the thermosyphon have been separately considered.

The prediction of the performance and the thermal behavior of a thermosyphon are mostly affected by the heat transfer in the evaporator and in the condenser sections that is usually with correlations and physical modeling. Regarding with the condenser the Nussel'ts approach is basically used to predict the condensing performances [1]. In 2001, Pan [17] developed an one-dimensional, steady state model that introduced the viscous force at the vapor-liquid film interface. The numerical results indicated that there exists a discrepancy between the Pan's model and Nusselt's solution especially in high confinement conditions. Harley and Faghri [18] in 1994

presented a model that coupled a general quasi-steady Nusselt type solution of the falling film with the complete two-dimensional vapor solution in order to simulate the transient behavior of TPCT without considering liquid pool. Jiao et al. [19] developed a new steady state model, based on experimental previous observations. They affirm that three types of flow pattern and two types of transition can be observed, according to the distribution of liquid film and liquid pool can be observed during the thermosyphon operations. The model is mainly based on the classical boiling Rosenhow's correlation. It accurate matches the experimental data and can be used to predict the effects of filling ratio on dryout, flooding and boiling limits. The real limit of this model it cannot simulate the unsteady violent boiling in the liquid pool that affects so much the thermosyphon performances. Recently, Shabgard et al. [20] numerically developed a two-dimensional model to simulate the transient operation of a TPCT with various filling ratios, defined as the ratio of charged liquid volume to the evaporator volume is one of the most important factors. This model is based on the model for the condensate previously developed by the author in 1994 [18]. This model has been compared with steady state experimental results with a good accordance. The authors used this model for finding the optimally filled thermosyphon that minimizes the thermal resistance. They affirm that the best thermosyphon is at optimal filling ratio with a small amount of additional working fluid. A critical point in the thermosyphon analysis is observed at the connection between the laminar condensation falling film and the upper level pool, because sometimes a local dryout condition has been numerically observed, however, this model has been validated only with steady-state experimental data and with filling ratio of 36% and 160%.

As just mentioned before, the heat transfer performance of a TPCT is significantly affected by geometry, inclination angle, vapor temperature and pressure, working fluid and mostly filling ratio affecting limitations and performances. For instance, in solar thermal applications, TPCT-solar thermal system is highly dependent on the filling ratio [21]. Selection of optimum filling ratio for solar thermal application is highly important, as during startup and operation at low heat fluxes, the oscillation phenomenon may occur. In the past the effect of filling ratio has been largely investigated. Payakaruk et al. [22] investigated the TPCT heat transfer performance by using different working fluids (R22, R123, R134a, ethanol, and water), at different filling ratios (50-100%), different orientations (5°-90°) and different ratios of evaporator length to diameter (5-40). They found that, the filling ratio has no effect on the ratio of heat transfer characteristics at any angle to that of the vertical position, but the properties of the heat transfer coefficient affected the heat transfer rate.

Park et al. [23] investigated experimentally the effect of filling ratio (10-70%) of a copper TPCT (D=22 mm) filled with FC-72 with a heat input ranged from 50 up to 600 W. They observed that for the small filling ratio (less than 20%), the critical limitation is the dryout, while for the large filling ratio (50%) the flooding limitation is occurred. Noie [24] experimentally analyzed the effects of filling ratio (30-90%), at different input heat rates (100-900 W), for a thermosyphon filled with water. He evaluated the optimum filling ratio at different evaporator lengths. Ong et al. [25] experimentally investigated a TPCT filled with R410a and water at different filling ratios (0.25-1), inclination angles (30˚-90˚) and power input (100–830 W). The results showed that the evaporator wall temperature was not uniform especially at high power input, low filling ratios and large inclinations. Abreu and Colle [26] presented the experimental analysis of the thermal behavior of TPCTs with different evaporator lengths (1000, 1350 and 1500 mm), filling ratios (60% and 80%), cooling temperatures (20˚C and 40˚C) and inclinations (30˚ and 45˚). They basically showed that an increase in filling ratio from 0.6 to 0.8 lead to increase in the evaporator temperature especially at high input heat fluxes.

This literature review shows that the filling ratios affect so much the heat transfer performances and the maximum heat flux of a thermosyphon. Even if a large number of experimental data at different operative and geometrical conditions has been presented the effect of filling ratio seems to be almost unclear. Some results appear contradictory among them especially on the dryout insurgence. The oscillation in the pool mass and the oscillating level can strongly influence the dryout insurgence, especially in case of small amount of liquid in the evaporator. In order to understand the effect of filling ratio a transient analysis of a thermosyphon must be absolutely made. From the literature it is found that the dryout limit in transient operation is few investigated, as well as the transient behavior of the liquid pool. To authors' knowledge, a joined numerical and experimental investigation of the thermal behavior of TPCTs under transient operation at low filling ratios has never been carried out. For this purpose, a transient 2-D numerical model is presented mainly based on the Shabgard et al. [20] approach. Furtherly a specific experimental setup has been designed aimed to understand the transient thermal behavior the thermosyphon at different filling ratios ranged from 16, 35 and 135%. A good accordance between the experimental and numerical data has found under transient operation. The experimental results joined with the mathematical model have allowed a dynamic analysis of the thermosyphon.

2. OPERATING PRINCIPLES AND METHODOLOGY

A TPCT consists of three different sections: an evaporator, a condenser and an adiabatic section (see **Fig. 1**). To determine the TPCT performance, it is worth describing the thermal-fluid phenomena inside it. In such a device, the input power is supplied through the evaporator wall to the working fluid and the liquid contained in the pool inside the evaporator starts to evaporate. Vapor flows upward inside the pipe up to the condenser where condenses at the inner pipe wall. Film condensation starts at the condenser inner walls and the film thickness highly affects the fluid dynamics of vapor flow in the core region. In the case of a low vapor velocity, the liquid film increases the thickness falling down counter currently to the vapor.

To design a TPCT, there is need to determine the working fluid filling ratio to maximize its performance while avoiding the dryout of the liquid film in the evaporator section. The minimum filling ratio that keeps the TPCT having a circulation of vapor and liquid film at a given heat input is called optimum filling ratio. When filling ratio is more than optimum one, the liquid film and liquid pool are continuous. However, when filling ratio is less than optimum, a film dryout in the evaporator could occur [19, 31]. It is considered in the numerical simulation that dryout limit is reached when the liquid pool is completely dried out (L_p=0). Depending heat flux and filling ratio, it is also possible to reach dryout in the liquid film above the liquid pool level (when the mass flow rate of liquid film goes to zero before reaching the surface of liquid pool): this phenomenon is referred to as local dryout. This can occur due to the effects of the high evaporation rate and interfacial shear, leads to prevent the down flow of liquid.

A high filling ratio of the working fluid, although avoiding liquid film dryout in the evaporator, could degrade the TPCT performance. Since the liquid film heat transfer coefficient is significantly higher than that of the liquid pool, as the liquid pool height in the evaporator increases (the liquid film length decrease) with increasing filling ratio, the effective conductance of the TPCT evaporator decreases. Another reason to find the optimum filling ratio is that a high filling ratio in some high temperature thermosyphons causes vibration of the thermosyphon due to geyser boiling [32-34]. Geyser boiling is an unstable phenomenon inside thermosyphon due to vapor that generates and expands suddenly due to hydraulic head reduction, and may cause vibration and damage of the pipes. The geyser boiling puts no limitation on thermal performance of thermosyphon, but it should be avoided because it damages the condenser end cap due to the slug impact.

It is clear that an optimum filling ratio selection could improve the system performance due to lower thermal resistances and response times. Therefore, the study of the thermal performance of the TPCT with a low filling ratio is a matter of interest and this paper presents numerical and experimental methodologies to evaluate heat transfer characteristics and operating limitations of a TPCT.

3. MATHEMATICAL MODEL

According the model proposed by Shabgard et al. [20] the thermosyphon has been basically divided into three different sections: liquid pool, falling film liquid and vapor core, as shown in **Fig. 2a**, as well as block diagram of numerical proceed (**Fig. 2b**).

For the model description convenience, the thermal-fluid phenomena occurring inside the working fluid are however divided into 4 different zones, namely: the vapor core, the metallic case, the pool and the laminar film. A transient two dimensional approach has been applied to the heat, mass and momentum balances for the case of vapor zone and the pipe wall. An one-dimensional quasi-steady approach has been used to simulated the liquid film and a the liquid pool. The model has been developed similarly to that of [20] in which there are some differences in the heat transfer correlations in the liquid pool as discussed in above section. The assumptions made in this analysis are: the condensate liquid film is quasi-steady, temperature distribution inside liquid film is linear, the liquid film thickness is so small (respect to vapor space), the vapor is an ideal gas, the condensate flow is one-dimensional (i.e. it lacks a radial velocity component), the condensate flow occurs at the working fluid saturation temperature, all thermophysical properties are constant, and expansion of the liquid pool due to the formation of vapor bubbles is neglected.

As first hypothesis the vapor is considered a compressible and laminar vapor flow with constant viscosity. The vapor space is a cylinder and the mass, momentum and energy equations in cylinder coordinates are considered, where *u* and *v* are the axial and radial velocity components, *V* is the velocity vector and Φ is the viscous dissipation term relative to the working fluid.

$$\frac{\partial \rho_v}{\partial t} + \frac{1}{r}\frac{\partial}{\partial r}(r\rho_v v_v) + \frac{\partial(\rho_v u_v)}{\partial z} = 0 \tag{1}$$

$$\rho_v \frac{DV_v}{Dt} = -\nabla P_v + \frac{1}{3}\mu_v \nabla(\nabla . V_v) + \mu_v \nabla^2 V_v \tag{2}$$

$$\rho_v c_{p,v} \frac{DT_v}{Dt} = \nabla . k_v \nabla T_v + \frac{DP_v}{Dt} + \mu_v \Phi \tag{3}$$

The heat transfer through the heat pipe wall is transferred by conduction, where ρ_w and $c_{p,w}$ are the density and specific heat of pipe material.

$$\rho_w c_{pw} \frac{\partial T}{\partial t} = k_w \left[\frac{1}{r} \frac{\partial}{\partial r} \left(r \frac{\partial T}{\partial r} \right) + \frac{\partial^2 T}{\partial z^2} \right] \tag{4}$$

The falling film along the wall has been modeled with a quasi-steady Nusselt type analysis. **Fig. 2a** shows a control volume inside the liquid film. For each control volume the mass, momentum and energy balances have been considered. The momentum equation balance aims to determine the hydrodynamic behavior of liquid film,

$$\frac{d^2 u_l}{dy^2} = \frac{1}{\mu_l} \frac{dP_l}{dz} + \frac{\rho_l g}{\mu_l} \tag{5}$$

Dealing with the mass term it is possible to affirm that the mass that enters in a liquid film fixed control volume can be due to different phenomena: the condensation/evaporation of vapor and liquid film from the upper volume, the mass flow rate of liquid film (Γ) (y direction) and the vapor mass condensation/evaporation rate per unit length along its width ($\dot{m}_v$) (radial direction), where the δ is the liquid film thickness, u_l is the axial liquid velocity, v_v is the radial vapor velocity

$$\Gamma = \int_0^{\delta} \rho_l u_l(y) dy \tag{6}$$

$$\dot{m}_v = \frac{d\Gamma}{dz} = \rho_{v,\sigma} v_{v,\sigma} \tag{7}$$

The liquid pool has been divided into several volumes where the mass and energy equation have been considered. The filling ratio of the working fluid in the evaporator section is determined from the overall mass balance in the thermosyphon. This mass balance accounts for the liquid film in the condenser, adiabatic, evaporator sections and liquid pool regions in the evaporator section and for the vapor in the thermosyphon cavity. The liquid pool temperature is determined by solving the heat conduction equation and the total liquid film mass and vapor mass inside the thermosyphon have been used to evaluate the liquid pool height (L_p) during the transient operations. As mentioned before at t=0, the initial height of the liquid pool can be obtained by considering that no liquid is along the wall.

The heat transfer mechanism at the evaporator section depends on the filling ratio and the heat flux. The condensation heat transfer coefficient in a TPCT is usually given by the falling film thickness according to Nusselt's correlation

$$h_{Nusselt} = 0.943\left\{\frac{\rho_l(\rho_l-\rho_v)gk_l^3\left[h_{fg}+0.68C_{pl}(T_v-T_c)\right]}{\mu_l(T_v-T_c)L_c}\right\}^{1/4} \tag{8}$$

Hashimoto and Kaminaga [27] found that the condensation heat transfer values are smaller than those calculated from the Nusselt theory, due to a confinement effect that makes more critical the vapor entrainment. Thus, they proposed a correlation taking into account the fact that at lower heat fluxes the film thickness is smaller, combined with the knowledge that the amount of entrainment increases as the density ratio increases (ρ_l/ρ_v),

$$h_c = 0.85\,\mathrm{Re}_f^{0.1}\exp\left(-0.000067\frac{\rho_l}{\rho_v}-f\right)h_{Nusselt} \tag{9}$$

where the *f* factor is due to the confinement effect and it is equal to 0.6. In 2010, Jouhara and Robinson [28] modified the *f* factor (*f*=0.14). For the evaporator the working fluid inside the evaporator shows three basic sections: the liquid pool, the liquid film and the upcoming vapor. Therefore, the heat transfer mechanism at the evaporator section could be more complex. Dealing with the liquid pool, different heat transfer regimes can be observed: single phase natural convection (at low heat fluxes), two-phase natural convection (at intermediate heat fluxes) and nucleate boiling (at high heat fluxes). According El-Genk and Saber [29], the occurrence of one of the different regimes depends on the complex combination of geometry, filling ratio and heat flux. Single phase natural convection is usually neglected. In this paper, the natural convection regime defined by

$$h_{nat} = 0.475\left(\frac{k_l}{L_p}\right)Ra^{0.35}\left(\frac{L_b}{d_i}\right)^{0.58} \tag{10}$$

According by El genk and Saber [29], the use of the classical correlations developed for unconfined boiling could generate errors, because they do not take into account the effect of local mixing along the heated wall between the rising bubbles. In order to select the most appropriate heat transfer correlation during operation El-Genk and Saber [29] proposed a criterion to define the heat transfer regime inside the pool, based on dimensionless parameter

$$X = \Psi\left(Ra \ \mathrm{Pr}_l\right)^{0.35}\left(\frac{P_v L_b q}{\sigma \rho_g h_{fg} \nu_l}\right)^{0.7} \tag{11}$$

where X is the dominant heat transfer regime and Ψ is the mixing coefficient. Heat transfer of the pool is dominated by natural convection if $X < 10^6$. Two-phase convection is considered if $10^6 \le X \le 2.1\times10^7$ while nucleate boiling is considered if $X > 2.1\times 10^7$. The criterion proposed in [29] is considered in this study, as well as two-phase convection correlation

$$h_{TPC} = 4\left(\frac{k_l}{d_i}\right)\left(ArFr^{0.5}\right)^{1/3}\mathrm{Pr}_l^{0.5}\left(\frac{Bo}{10}\right)^n,\ n=\begin{cases}1/2, \text{For} & Bo \le 10\\ 1/6, \text{For} & Bo \ge 10\end{cases},\ 10^6 \le X \le 2.1\times 10^6 \tag{12}$$

The correlation defined by Imura et al. [30] is used to predict the nucleate boiling regime, as will be shown later; Imura correlation [30] can predict the measured values in reasonable agreement

$$he = 0.32\left(\frac{\rho_l^{0.65} k_l^{0.3} C_{pl}^{0.7} g^{0.2}}{\rho_v^{0.25} h_{fg}^{0.4} \mu_l^{0.1}}\right)\left(\frac{P_v}{P_{atm}}\right)^{0.3} q^{0.4} \tag{13}$$

Concerning applied boundary conditions (see Fig. 2a), at the centerline, the radial vapor velocity, the radial gradients of axial velocity and the radial gradients of temperature are all considered equal to zero. At both ends of the thermosyphon (bottom and upper cap) the no-slip condition for velocity field and the adiabatic condition for temperature field are applied. Concerning interface boundary conditions, at the liquid film-wall interface, at any axial position above the pool, the heat flux into and output of wall is given by

$$-k_s \frac{\partial T_w}{\partial r} = \frac{(T_s - T_w)}{R_{film}},(r=r_i,\ \delta>0,\ L>L_p) \tag{14}$$

where $R_{film}=\delta/kl$ is the thermal resistance of the liquid film in the all the section except for the condenser section. In this paper, the film thickness thermal resistance in the condenser section has been taken equal to that proposed by [35].

If the liquid the film thickness above the pool is equal to zero, the thermosyphon is in local dryout condition. In this case, it is considered no evaporation and condensation and that the local vapor velocities close the hot surface is negligible. The temperature field is given by

$$k_w \frac{\partial T_w}{\partial r} = k_v \frac{\partial T_v}{\partial r}\text{, at } r=r_i \text{ and } \delta=0 \tag{15}$$

The governing equations are solved by using the control volume finite difference approach described by

Patankar [35]. A combination of direct method and the Gauss-Siedel method has been applied to solve the equations. The SIMPLER algorithm [35] is used to solve the differential balance equations described before. A code written in FORTRAN language was developed to numerically solve the problem by using a structured staggered and non-uniform grid system. Grid independence by the code was investigated by varying the number of axial and radial grids. The minimum values for grid size is 14×80 (r–z). The converged solution is assumed to be reached when the relative change of the velocity, pressure and temperature is less than 10^{-6}. Concerning the initial conditions, the temperature of the TPCT has been considered equal to the environmental temperature and the initial pressure is set to be equal to the saturation pressure at the initial temperature.

4. EXPERIMENTAL PROCEDURE

4.1 Experimental apparatus

In order to dynamically evaluate the thermal performances and the operating limitations of a TPCT a specific experimental setup has been designed and realized.

The experimental system consists of: the cooling flow loop, the test cell and the control and acquisition systems (Fig. 3).

The TPCT is made of a smooth copper pipe with a 35 mm outer diameter 500 m long and 1 mm thick, The thermosyphon is closed at the ends with two 3 mm thick copper caps. The evaporator section is uniformly heated by using silicon thermofoil heater, 75 mm long, (model MINCO HK5488R17.2L12A) clamped to the external evaporator wall surface. Heaters and blocks were covered with several layers of polymer insulation to minimize heat loss from this section. The power input is supplied by a DC Power supply (Agilent DC6575A) with a maximum power output of 700 W which has an accuracy of ±1 percent of reading.

The condenser is cooled by, water coming from a cooling bath (HAKKE F-3C DIN 58966). It consists of a 150 mm long copper pipe mounted around the TPCT, with an outside diameter of 42 mm and a wall thickness of 1.25 mm. An electromagnetic flow meter (Siemens SITRANS F M MAGFLO5000) allows the mass flow rate measurement of the cooling water with an accuracy of about 1%. Two thermocouples in located at the condenser inlet and outlet and the mass flow rate measurement allow to calculate the cooled by

condenser section to be calculated. **Table 1 and Table 2** list the detailed specification and operating parameters of the TPCT.

All the TPCT wall temperatures were measured using eleven T-type thermocouples, which have been calibrated with an accuracy of ±0.2˚C. The thermocouples (T_1 to T_{11}) mounted along the wall in the evaporator, adiabatic and condenser sections are shown schematically in **Fig. 3**. In the evaporator end cap, a pressure transmitter (PTX7511 accuracy of ±0.15%) is installed to measure vapor pressure. All the signals to monitor TPCT temperature and pressure and cooling mass flow rate are acquired by the Agilent HP32790 data acquisition system, and stored in a computer. To evaluate of the effect of filling charge of fluid on the performance of the TPCT, experiments were performed with a fluid charge of 10 to 85 ml of degassed, ultra-pure water, which this corresponded to a filling ratio from 16% to 135%.

4.2. Experimental procedure, data reduction and uncertainty analysis

The experiments were performed with the TPCT in the vertical position. As each run starts the cooling water temperature is set and all the systems is keep at the condensing temperature before the power supplying. Then, input power is set to the starting value with a step heating and the dynamic behavior can be observed up to a steady state regime, afterwards the input power is set the next step The temperature of the input and output cooling water and the outside thermosyphon walls along the axial length is measured over time. In the data analysis, the average heat transfer rate into the evaporator output of condenser section was applied. The measured variables in the experimental analysis are: heat rate applied to the evaporator section (Q_{in}), heat output of the condenser section (Q_{out}) temperature of inlet (T_{in}) and outlet of coolant water (T_{out}), mass flow rate of the coolant water (m), wall surface temperatures and vapor pressure. From the measured data of wall temperature and vapor temperature (equivalent to the wall temperature of adiabatic section), the heat transfer coefficient in the evaporator (h_e) and condenser section (h_c) can be evaluated using the following equations:

$$h_e = \frac{Q_{av}}{\pi d_i L_e (T_{e,ave} - T_v)} \tag{16}$$

$$h_c = \frac{Q_{av}}{\pi d_i L_c (T_v - T_{c,ave})} \tag{17}$$

where $T_{,e,ave}$ and $T_{c,ave}$ are average evaporator wall temperature (T_1, T_2 and T_3) and average condenser wall temperature (T_{10} and T_{11}), respectively, T_v is average adiabatic temperature and Q_{av} is average input

The rate of heat removal from the condenser section is calculated from the following relation:

$$Q_{av} = \dot{m} C_p (T_{out} - T_{in}) \tag{18}$$

The experimental uncertainties of the various parameters: heat input, thermal resistance and heat transfer coefficients are calculated. The relative experimental uncertainty can be described for the variable $R = R(x_1, x_2, \ldots, x_n)$ as:

$$\frac{U_R}{R} = \sqrt{\sum_{i=1}^{n} \left(\frac{x_i}{R} \frac{\partial R}{\partial x_i} \right)^2 \left(\frac{P_i}{x_i} \right)} \tag{19}$$

where P is the bias limit of the variable R. From above equations and mentioned uncertainty of apparatus, the relative uncertainties of the output heat flux from condenser section is estimated between 6.8% for low input power and improved to 4.8% for the higher power settings.

5. RESULTS AND DISCUSSION

5.1. Transient behavior of the TPCTs

A set of tests and numerical simulations were performed to investigate the thermal performance of the TPCT under normal and operating limitations (dryout and geyser boiling oscillation) at varying filling ratios and heat fluxes. The overall thermal resistance, evaporation and condensation heat transfer coefficients of the TPCT are also evaluated.

Before introducing the steady state operation of thermosyphon at different filling ratios, the transient behavior of the system is thermosyphon from normal to limiting operation at two filling ratios. **Fig. 4** shows the average wall temperature variation of evaporator, adiabatic and condenser sections as well as output heat flux from condenser section at the heat flux ranged 30 to 700 W and filling ratio of 16%. The zero of time is taken as the certain moment at which the output power was increased. It is found that the normal operation continues up to heat transfer rate of 600 W. With increasing heat flux, the wall temperature at the evaporator section starts to increase suddenly due to dryout, the heater is switched off.

In other case, **Fig. 5** shows the evaporator (T_2 and T_3) condenser and adiabatic variation temperature over time for input power steps from 30 up to 700 W at filling ratio of 35%. The trend of Q_{out} is also shown in **Fig. 5**. Constant low temperatures at the evaporator wall are observed from 30 W up to a 150 W. As the input power is gradually increased the temperatures T_2 and T_3 start to raise. It should be noted that based on filled charge, for non-operating thermosyphon, the temperature T_2 lie within the liquid pool area. It is observed that from heat flux of 200 up to 350 W the upper evaporator end is dried, no more liquid flows into the liquid pool and the pool level is reduced. This leads to a local dryout, T_2 and T_3 is increasing. With increasing heat flux from 350 W to 400 W, a large oscillation is noted. The temperature oscillations could be explained by geyser boiling. The temperature of low pressure falling liquid to the evaporator increases, hence under this condition suddenly vaporizes and causes to a large vapor slug grows in the subcooled liquid and violently pushes the above liquid column up to the condenser, the pressure increase and the temperature decreases. It is due to the liquid motion inside the pool. Fig. 6 confirms this hypothesis. A small temperature fluctuations is observed at the condenser section (2.5 °C) and rather high at the evaporator section (62 °C). The high temperature oscillation could be due to high local superheating.

Results for a typical case at low heat transfer rate and high filling ratio (135%) is evidenced in Fig. 7 for the temperature variations of the evaporator (T2), adiabatic (T6) and condenser (T10) wall, as well as output heat flux from condenser section. A qualitative trend of the geyser boiling phenomena is evidenced in the initial stage of operation at heat transfer rate of 30 W while the thermosyphon can operate under normal operation at higher heat flux. It is clearly observed that the condenser stayed at a low temperature, except when some liquid was pushed up by the growing bubble from the evaporator to the condenser. The zigzag temperature variation is indicated in a close illustration evidenced in Fig. 7.

The obtained results from above transient analysis at different filling ratios suggest that the thermal performance of the tested thermosyphon highly depends on filling ratio and heat flux. It is confirmed that at filling ratio of 16% thermosyphon operates normally at different heat loads while as fluid charge increases to 35% and 135% the geyser boiling is experienced. The period of oscillation strongly depends on filling ratio and heat load. The situation is completely different for a filling ratio of 35% and 135%. In case of filling ratio of 35% dryout starts from heat load of 200 W and temperature oscillation occurs at heat transfer rate of 400 W, while geyser boiling occurs at first stage of operation (Q=30 W) for filling ratio of 135%.

5.2. Steady state behavior of TPCTs

Concerning steady state thermal behavior of TPCTs, the experimental data are compared over time with the numerical data given by model at different filling ratios: 16%, 35% and 135%. **Fig. 8** shows the outer copper pipe temperatures along the Z-axis at different times (t=0, 20, 40, 60, 90s and steady state operation) in case of an input power of 100 W and filling ratio of 16%. The different colored marks are referred to the experimental data and the different colored lines to the numerical data. **Fig. 8a** shows that the temperature increases over time in the evaporator and the condenser section during the early transient operations. A wall temperature overshoot can also be observed in the region immediately above the liquid pool level in evaporator section. This overshoot reaches a maximum at 60 s in the experimented case because no liquid film is at the walls and it is a similar behavior that can be found as a local transient dryout occurs. Even if at the steady state regime the temperature along the axis is almost constant, the local dryout insurgence could be dangerous for the device. This phenomenon is mainly due to the effects of the high evaporation rate and the interfacial shear that prevent to the liquid film of flowing down. The condensate film reaches the steady condition at t=150s.

The experimental and numerical results at steady state operation indicated that the temperature distribution of the thermosyphon is nearly uniform in evaporator section and decreases slightly towards the adiabatic section. The temperature reaches the minimum value at the bottom part of the condenser section.

Numerical and experimental transient variation of temperature distribution at filling ratios of 35% and 135% are shown in **Figs. 8b and 8c**. It is clearly evidenced that at filling ratio of 35% the maximum overshooting temperature is about 5°C lower than that relative to a filling ratio of 16% even if the average evaporator temperature at steady state is higher. In the case of quite large filling ratio (135%), none local dryout is observed even if the highest evaporator temperature is found. It is worth noticing at low filling ratio the thermal resistance is really better than the other cases, but is easier find local conditions with high temperature overshooting. It is therefore easier that the system finds a thermal crisis at lower input power. In all the tested cases, a good agreement between numerical and experimental data is observed at different filling ratios under normal operation.

Figs. 9a and b show the experimental and numerical wall temperatures along the thermosyphon at low filling ratio, close to the dryout occurrence (filling ratio=16%). At the middle part of evaporator section, it

can be noticed that experimental temperature starts to increase and at t=20 s reaches a local temperature of 100 °c about and afterwards the dryout occurs. The numerical temperature distributions have been plotted at the same time step in **Fig. 9b**. It is important to note that at time t=20 s the model is able to predict the local superheating of 100°C about but as the time goes on the thermosyphon evolves towards a steady state operation instead of the dryout occurrence. The liquid film dryout experimentally has been observed at a power input of 650 W and why the model is not to able to predict it. It seems that close to dryout occurrence the liquid vapor interface probably becomes wavy, the liquid/vapor shears force raise up and the liquid returning from the condenser could be insufficient to replenish the liquid pool in the evaporator. The liquid pool height decreases; therefore, the length of the liquid film in the evaporator becomes progressively thinner. As a result, the liquid film thickness in the evaporator, immediately above the liquid pool reaches a critical value and it breaks ups into small rivulets separated by dry patches [31]. However, this kind of liquid film dryout could not predict by numerical simulation, as the dryout is occurred when the liquid pool length is zero.

The optimal filling ratio obtained by numerical simulation is 10% (**Fig. 10**). As discussed in section 2, in this paper the optimal filling ratio corresponds to a condensate film extending from the condenser end cap to the evaporator end cap at steady state operation. From above discussion and analysis, it could be confirmed that the presented numerical simulation can predict the thermal behavior of thermosyphon at normal operation. It should be noted that a very accurate validation of numerical model at critical filling ratio can not be obtained. This could be due to the fact that the numerical model can predict the dryout limitation when all the liquid pooled in the bottom of evaporator section is vanished.

5.3. Heat transfer analysis

The heat transfer behavior of a thermosyphon is well described by the thermal resistance analysis. The thermal resistance versus the power input is shown in **Fig. 11** for different filling ratios (16%, 35% and 135%). It is clear that at low input powers all cases show a similar qualitative trend; thermal resistance decrease as the input power increases. At input power higher than 400 W, the thermal resistances are almost constant. At low filling ratio (16%) the thermosyphon shows a lower thermal resistance in comparison with those relative higher filling ratios (filling ratio= 35% and filling ratio=135%). On the other hand if

thermosyphon filled with high percentage of fluid does not found any heat transfer limitation, a dryout limitation at 700 W has been observed in the case of filling ratio=16%. The increase in the thermal resistance for filling ratio of 35% at heat transfer ranged from 200 up to 400 W is basically due to geyser boiling, as described in above section. The thermal performances of the thermosyphon with lower filling ratio (16%) is found to degrade significantly for power levels exceeding approximately 600 W. This is determined to be a result of reaching the thermosyphon operating limit.

The comparison between the calculated and measured heat transfer coefficient at the evaporator and condenser section are shown in **Fig. 12** and **Fig. 13**, respectively. As it is evidenced in **Fig. 12**, at heat transfer rate of about 30 to 600 W the heat transfer coefficient was about 1.6 –7 $kW/m^2 K$. It is observed that the Imura correlation is able to accurately predict the heat transfer inside the pool as expected from the literature for high filling ratios, but it seem not be able to predict the heat transfer at low filling ratios and as a violent geyser boiling is observed. The worse agreement is observed in the case of dryout and oscillation limitation, as evidenced in the **Fig. 12**. On the other hand the correlation used for the condenser section in [35] is accurate in comparison of the experiment data (see Fig.13). In authors' opinion there is need to investigate also the effect of evaporator length to confirm the accuracy of this correlation.

Lastly, from above analysis, it is confirmed that thermosyphons have better performances at lower filling ratios. At low filling ratios, however, a higher risk of thermal crisis or non performing geyser boiling oscillations is really possible. This analysis confirms that the heat transfer correlations are not being able to match the experimental data in these particular conditions. A transient analysis is therefore necessary in order to understand the real behavior of the thermosyphon at low filling ratios. This can help in the optimum filling ratio detection.

The experimental results show that the dryout is due to liquid film drying immediately above the surface of the liquid pool where a sudden increasing in the temperature has observed. According the numerical analysis the dryout is due to the drainage of all the liquid in the pool. It is also observed oscillations in the temperature, vapor pressure and output heat flux in a heat flux ranged 200 to 400 W at filling ratio of 35% hence, degrading the performance of the thermosyphon during transient operation with increasing heat flux. The limiting heat fluxes corresponding to the critical heat fluxes in the evaporator occur at low as well as at high liquid fillings depending on the input heat flux distribution. It is observed that the thermal resistance

decreases for the lowest fill ratio, but it is necessary to take care about dryout and geyser boiling oscillations which are very important to avoid in practical applications. In case of high fill charge (herein 35%) when the temperature is low and therefore the pressure is low, it may occur a transient oscillation where the evaporator temperature is not stable. Finally, by considering the appropriate filling ratio, a sustainable operation is possible in the TPCT mode. It should be noted that the above results and discussions are presented for a constant operating condition in the condenser section (cooling temperature and mass flow rate).

6. CONCLUSIONS

The paper describes an experimental and numerical analysis of a Two-Phase Close Thermosyphon at different filling ratios. The copper thermosyphon (ID=33 mm) is 500 mm long and is filled with water. The effects of the filling ratio on the heat transfer characteristics under normal and limiting operating conditions is investigated in the input heat transfer range of 30W<Q<700W and filling ratio of 16%<filling ratio<135%. The thermosyphon investigated in this paper shows the better performance for filling ratio lower than 35%. At this filling ratio a major risk of dryout insurgence or a non performing geyser boiling can be found. By comparing the experimental data with a 2-D mathematical model a good accordance has been observed. In particular the model is able to predict the transient axial temperature trend even in critical conditions (dryout). The model is also able to predict the heat and mass transfer in the liquid pool and in the zone where the film of condensate liquid is absent.

From the experimental data, it is found that at small filling ratio (filling ratio= 16%), the heat transfer is limited by the dryout of falling liquid film in the zone immediately above the liquid pool. It has been found at 650 W (8,3 kW/m2). The geyser boiling is also observed at filling ratio of 35% and 135% at first stage of operation (Q=30 W) and from 200 to 400 W, respectively.

According to the numerical model the dryout of the falling liquid film close to the liquid pool is only a transient temperature overshooting because the system is able to reach a steady state regime afterwards. Numerically speaking the dryout can be found only if the liquid pool it is totally dried. At the same heat fluxes the model predict a dryout if the Filling ratio is 10%. In order to better predict the behavior of thermosyphon at low filling ratio, a better heat transfer characterization must be done in order to better simulate the thermosyphon behavior at really low heat flux.

NOMENCLATURE

Ar : Archimede number

Bo : Bond number

C : Specific heat (J/kg K)

D : Diameter (m)

Fr : Froude number

H : Heat transfer coefficient (W/m^2K)

h_{fg} : Heat of vaporization (J/kg)

K : Thermal conductivity (W/mK)

L : Length (m)

M : Mass (kg)

$\dot{m}$: Mass flow rate (kg/s)

Nu : Nusselt number, *hL/k*

P : Pressure (Pa)

Q : Heat transfer rate (W)

Q : Heat flux (W/m^2)

R : Thermal resistance (K/W)

R : Radius (m)

Ra : Rayleigh number

Re : Reynolds number, $4Q/\pi Dh_{fg}\pi$

T : Time (s)

T : Temperature (K)

V : Velocity vector(m/s)

U : Axial velocity inside the liquid film (m/s)

V : Velocity (m/s)

Y : Axial coordinate ins. the liquid film (m)

Z : Axial coordinate (m)

Greek symbols

β : Inclination angle ($^{\circ}$)

δ : Liquid film thickness (m)

Γ : Mass flow rate of liquid film

Φ : Dissipation term Eq (3)

ν : Kinematic viscosity (m^2/s)

ρ : Density (kg/m^3)

μ : Dynamic viscosity (Pa s)

σ : Surface tension (N/m)

Subscripts

A : Adiabatic

C : Condenser

E : Evaporator

Eff : Effective

I : Inner wall

L : Liquid

Max : Maximum

Min : Minimum

O : Outer

P : Pool

T : Total

V : Vapor

REFERENCES

[1] D.A. Reay, P. Kew, Heat Pipes, 5th ed. Oxford, UK: Butterworth-Heinemann, (2006).

[2] A. Faghri, Heat Pipe Science and Technology. Philadelphia, PA: Taylor & Francis, (1995).

[3] S. Filippeschi, Comparison between miniature periodic two-phase thermosyphons and miniature LHP applied to electronic cooling equipment, App Therm Eng 31 (2011) 795-802.

[4] G. P. Peterson, Heat Pipes, Modeling, Testing, and Applications. John Wiley and Sons, (1994).

[5] L.L. Vasiliev, S. Kakaç, Heat Pipes and solid sorption transformations Fundamentals and Practical Applications, Ed. CRC Press- Taylor & Francis Group (2013).

[6] D. Jafari, A. Franco, S. Filippeschi, P. Di Marco, Two-phase closed thermosyphons: A review of studies and solar applications, Ren Sust Energy Reviews 53 (2016) 575–593.

[7] M. A. Hakeem, M. Kamil, I. Arman, Prediction of temperature profiles using artificial neural networks in a vertical thermosiphon re-boiler, Appl Therm Eng 28 (2008) 1572–1579.

[8] Y. Cao, M. Gao, Wickless network heat pipes for high heat flux spreading applications, Int J Heat Mass Transf 45 (2002) 2539–2547.

[9] S. Siedel, A. J. Robinson, R. Kempers, S. Kerslake, Development of a naturally aspired thermosyphon for power amplifier cooling, J Phys Conf Ser 525 (2014) 012007.

[10] M. E. Poulad, A. Fung , Potential benefits from Thermosyphon-PCM (TP) integrated design for buildings applications in Toronto, In: Proceedings of eSim: The Canadian Conference on Building Simulation 601 (2012) 601-614.

[11] M. Zhang, Y. Lai, J. Zhang, Z. Sun, Numerical study on cooling characteristics of two-phase closed thermosyphon embankment in permafrost regions, Cold Reg Sci Technol 65 (2011) 203–210.

[12] S. Tundee, N. Srihajong, S. Charmongkolpradit, Electric power generation from solar pond using combination of thermosyphon and thermoelectric modules, Energy Proc 48 (2014) 453–463.

[13] P. Byrne, J. Miriel, Y. Lénat, Experimental study of an air-source heat pump for simultaneous heating and cooling – part 2: dynamic behavior and two-phase thermosiphon defrosting technique, Appl Therm Eng 88 (2011) 3072–3078.

[14] F. Dobran, Steady-state characteristics and stability thresholds of a closed two-phase thermosyphon, Int J Heat Mass Transfer, 28 (1985) 949-957.

[15] A. F. Vieira da Cunha, M. B. H. Mantelli, Analytical and experimental analysis of a high temperature mercury thermosyphon, J Heat Transfer 131 (2009) 1-7.

[16] B. M. Ziapour, H. Shaker, Heat transfer characteristics of a two-phase closed thermosyphon using different working fluids, Heat Mass Transfer 46 (2010) 307–314.

[17] Y. Pan, Condensation heat transfer characteristics and concept of sub-flooding limit in a two-phase closed thermosyphon, Int Commun Heat Mass Transfer 28 (2001) 311–322.

[18] C. Harley, A. Faghri A, Complete transient two-dimensional analysis of two-phase closed thermosyphons including the falling condensate film, J Heat Transfer 116 (1994) 418-426.

[19] B. Jiao, L. M. Qiu, Z. H. Gan, X. B. Zhang, Determination of the operation range of a vertical two-phase closed thermosyphon, Heat Mass Transfer 48 (2012) 1043-1055.

[20] H. Shabgard, B. Xiao, A. Faghri, R. Gupta, W. Weissman, Thermal characteristics of a closed thermosyphon under various filling conditions, Int J Heat Mass Transfer 70 (2014) 91–102.

[21] H. M. S. Hussein, H. H. El-Ghetany, S. A. Nada, Performance of wickless heat pipe flat plate solar collectors having different pipes cross sections geometries and filling ratios, Energy Convers Manag 47 (2006) 1539-1549.

[22] T. Payakaruk, P. Terdtoon, S. Rittidech, Correlations to predict heat transfer characteristic of an inclined closed two-phase thermosyphon at normal operating conditions, Appl Therm Eng 20 (2000) 781–790.

[23] Y. J. Park, K. H. Kang, C. J. Kim, Heat transfer characteristics of a two-phase closed thermosyphon to fill charge ratio, Int J Heat Mass Transf 45 (2002) 4655–4661.

[24] S. H. Noie, Heat transfer characteristics of a two-phase closed thermosyphon, Appl Therm Eng 25 (2005) 495–506.

[25] K. S. Ong, W. L. Tong, J. S. Gan, N. Hisham, Axial temperature distribution and performance of R410 and water thermosyphon at various fill ratios and inclinations, Front Heat Pipes 5 (2014) 2.

[26] S. L. Abreu, S. Colle, An experimental study of two-phase closed thermosyphons for compact solar domestic hot-water systems, Solar Energy 76 (2004) 141-145.

[27] H. Hashimoto, F. Kaminaga, Heat transfer characteristics in a condenser of closed two-phase thermosyphon: effect of entrainment on heat transfer deterioration, Heat Transfer-Asian Res 31 (2002) 212–225.

[28] H. Jouhara, A. J. Robinson, Experimental investigation of small diameter two phase closed thermosyphons charged with water, FC-84, FC-77 and FC-3283, App Therm Eng 30 (2010) 201–211.

[29] M. S. EL-Genk, H. H. Saber, Heat transfer correlations for small, uniformly heated liquid pools, Int J Heat Mass Transf 41 (1998) 261–274.

[30] H. Imura, K. Sasaguchi, H. Kozai, Critical heat flux in a closed two-phase thermosyphon, Int J Heat Mass Transfer 26 (1983) 1181–1188.

[31] M.S. EL Genk, H. H. Saber, Determination of operation envelopes for closed two-phase thermosyphons, Int J Heat Mass Transf 42 (1999) 889-903.

[32] T. F. Lin, W. T. Lin, Y. L. Tsay, J. C. Wu, Experimental investigation of geyser boiling in an annular two phase closed thermosyphon, Int J Heat Mass Transf 38 (1995) 295–307.

[33] H. Kunkoro, Y. F. Rao, K. Fukuda, An experimental study on the mechanism of geysering in a closed two phase thermosyphon, Int J Multiphase Flow 21 (1995) 1243–52.

[34] I. Khazaee, R. Hosseini, S. H. Noie, Experimental investigation of effective parameters and correlation of geyser boiling in a two-phase closed thermosyphon, Appl Therm Eng 30 (2010) 406–12.

[35] S. V. Patankar, Numerical Heat Transfer and Fluid Flow, Hemisphere, Washing. DC (1980).

Figures

Fig. 1 Schematic view of a TPCT.

Fig. 2 (a) Configuration of a TPCT, as well as boundary conditions and (b) procedure of mathematical model.

Fig. 3 Experimental setup scheme and thermocouples locations.

Fig. 4 Transient variations of the evaporator, adiabatic and condenser temperatures and output heat flux from the condenser section at different heat fluxes (filling ratio=16%).

Fig. 5 Transient variations of the evaporator, adiabatic and condenser temperatures and output heat flux from the condenser section at different heat fluxes.

Fig. 6 Transient evaporator temperature and vapor pressure variation of thermosyphon at the geyser boiling phenomena.

Fig. 7 Transient variations of the evaporator, adiabatic and condenser temperatures and output heat flux from the condenser section at different heat fluxes.

Fig. 8 Comparison of the experimental and numerical axial outer wall temperature at different time steps, Q=100 W: a) filling ratio=16%, b) filling ratio=35% and c) 135%

Fig. 9 Axial outer wall temperature at different time steps, Q=650 W and filling ratio=16%: a) Experimentally and b) Numerically.

Fig. 10 Numerical axial outer wall temperature at different time steps, filling ratio=10%, Q=800 W.

Fig. 11 Experimentally determined overall thermal resistance values.

Fig. 12. Comparison between the heat transfer coefficients experimentally and numerically evaluated in the evaporator section, Imura.

Fig.13 Comparison between the heat transfer coefficients experimentally and numerically evaluated in the condenser.

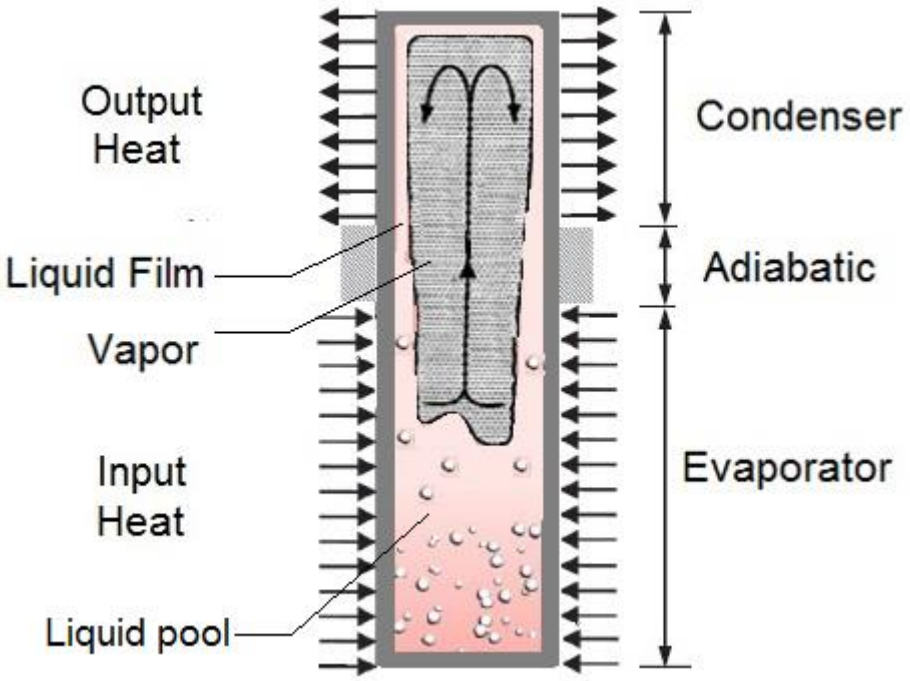
Output Heat
Liquid Film
Vapor
Input Heat
Liquid pool
Condenser
Adiabatic
Evaporator

Fig. 1

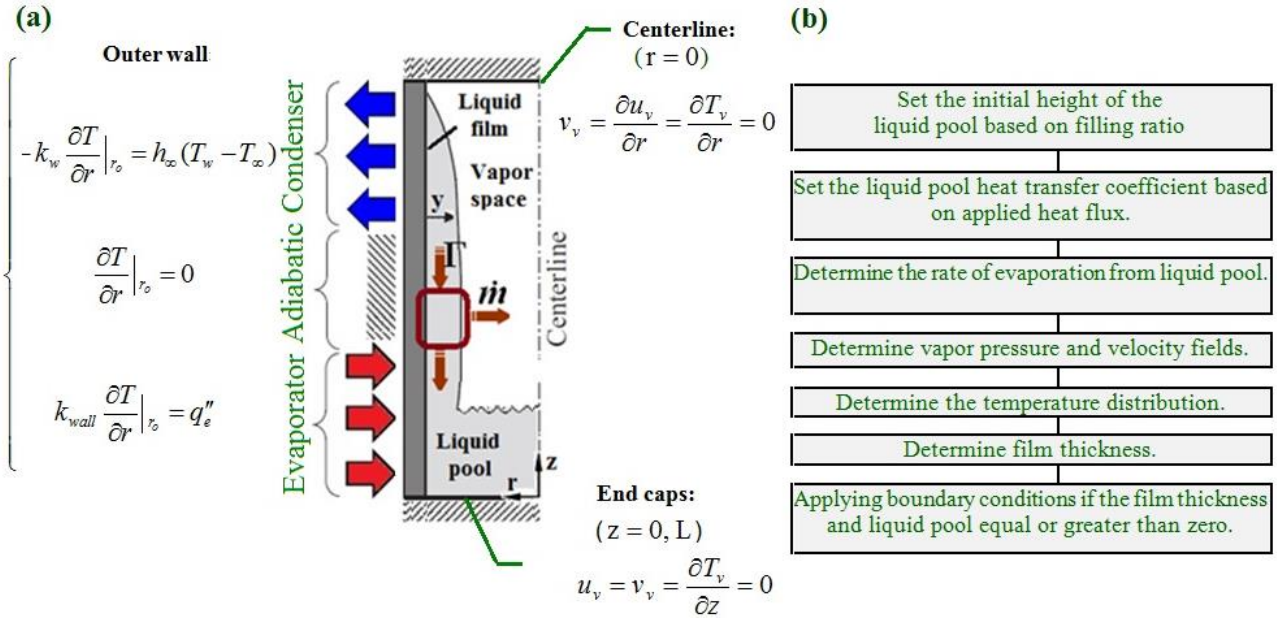
(a)
Outer wall
$-k_w \frac{\partial T}{\partial r}\Big|_{r_o} = h_\infty (T_w - T_\infty)$
$\frac{\partial T}{\partial r}\Big|_{r_o} = 0$
$k_{wall} \frac{\partial T}{\partial r}\Big|_{r_o} = q''_e$
Evaporator Adiabatic Condenser
Liquid film
Vapor space
y
Centerline
Liquid pool
r
z
Centerline:
(r = 0)
$v_v = \frac{\partial u_v}{\partial r} = \frac{\partial T_v}{\partial r} = 0$
End caps:
(z = 0, L)
$u_v = v_v = \frac{\partial T_v}{\partial z} = 0$
(b)
Set the initial height of the liquid pool based on filling ratio
Set the liquid pool heat transfer coefficient based on applied heat flux.
Determine the rate of evaporation from liquid pool.
Determine vapor pressure and velocity fields.
Determine the temperature distribution.
Determine film thickness.
Applying boundary conditions if the film thickness and liquid pool equal or greater than zero.

Fig. 2

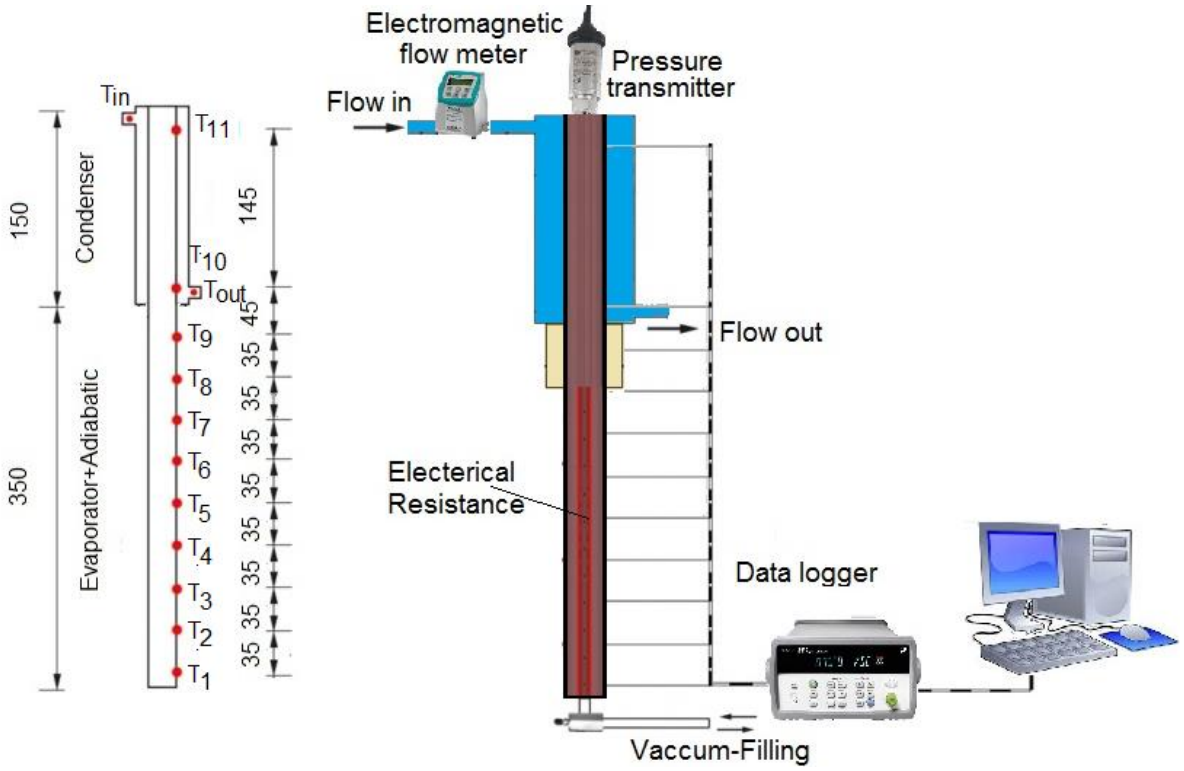
Electromagnetic
flow meter
Pressure
transmitter
Flow in
Flow out
Tin
T11
T10
Tout
T9
T8
T7
T6
T5
T4
T3
T2
T1
150
Condenser
350
Evaporator+Adiabatic
145
45
35
35
35
35
35
35
35
Electerical
Resistance
Data logger
Vaccum-Filling

Fig. 3

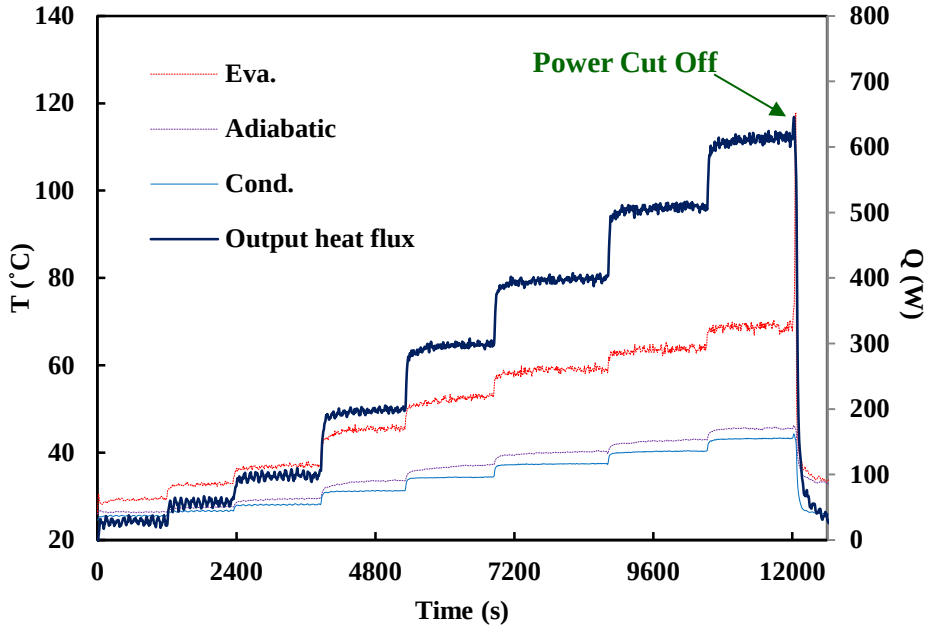
Power Cut Off
Eva.
Adiabatic
Cond.
Output heat flux
T (°C)
Q (W)
Time (s)
140
120
100
80
60
40
20
800
700
600
500
400
300
200
100
0
0
2400
4800
7200
9600
12000

Fig. 4

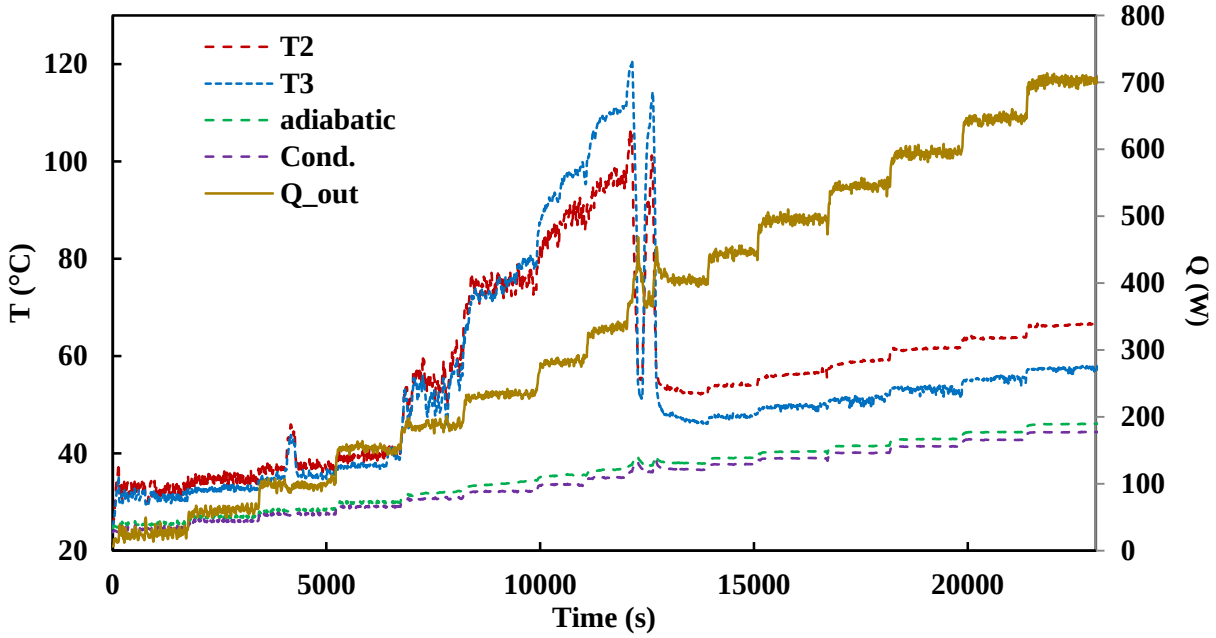
T2
T3
adiabatic
Cond.
Q_out
T (°C)
Q (W)
Time (s)
120
100
80
60
40
20
800
700
600
500
400
300
200
100
0
0
5000
10000
15000
20000

Fig. 5

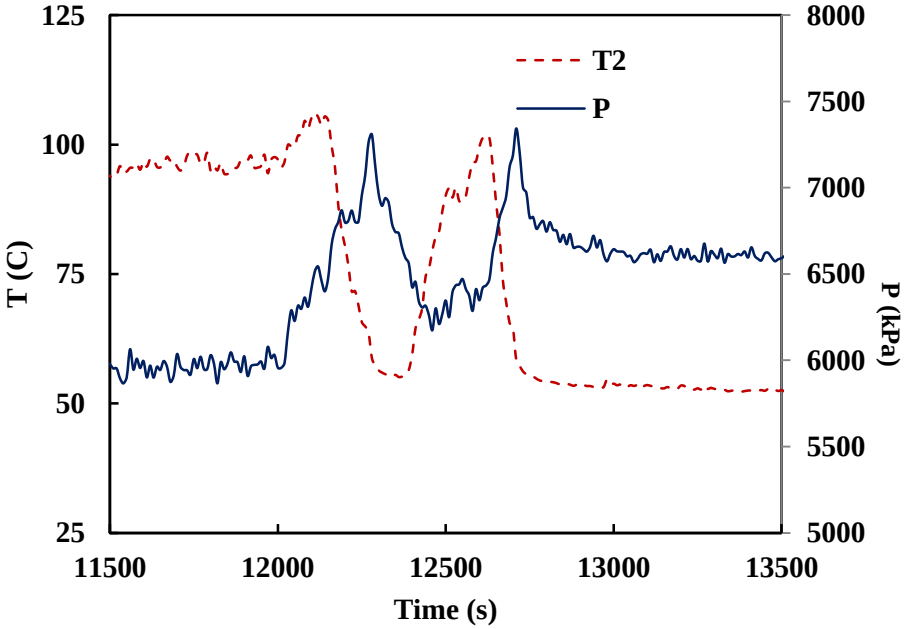
T2
P
T (C)
P (kPa)
Time (s)
125
100
75
50
25
8000
7500
7000
6500
6000
5500
5000
11500
12000
12500
13000
13500

Fig. 6

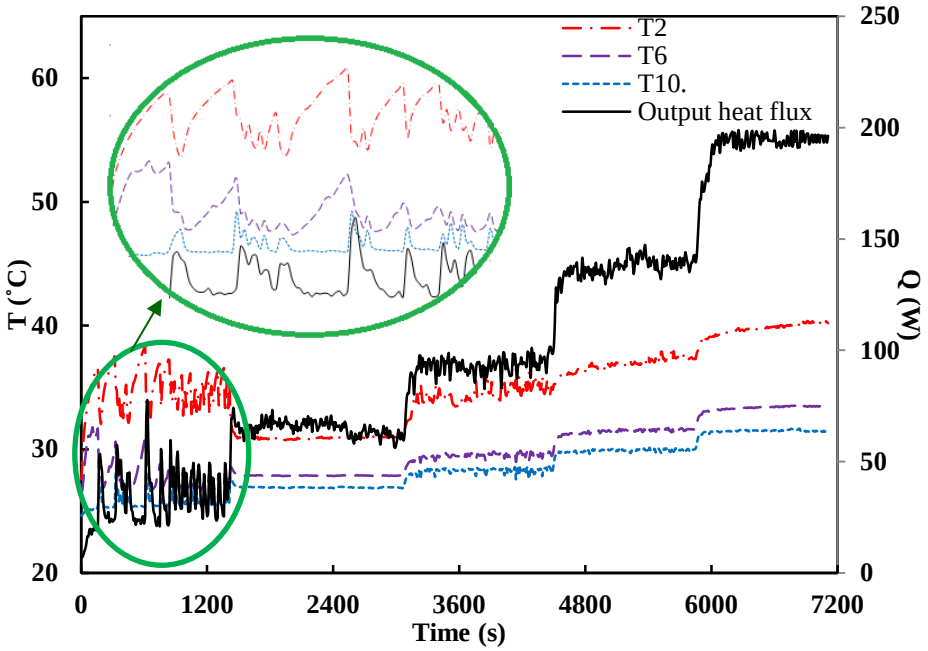
T2
T6
T10.
Output heat flux
T (°C)
Q (W)
Time (s)
20
30
40
50
60
0
50
100
150
200
250
0
1200
2400
3600
4800
6000
7200

Fig. 7

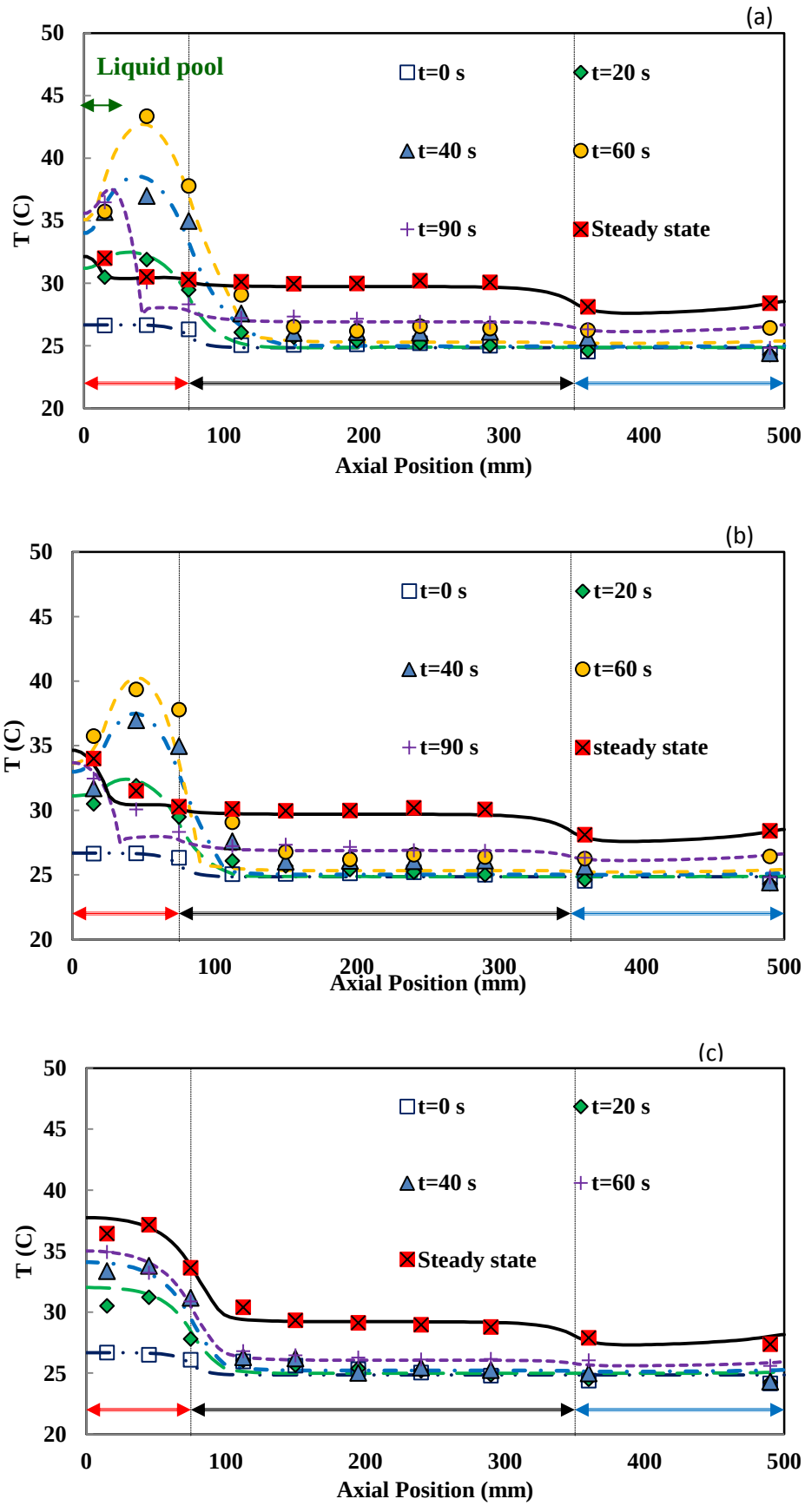
(a)
Liquid pool
t=0 s
t=20 s
t=40 s
t=60 s
t=90 s
Steady state
T (C)
Axial Position (mm)
(b)
t=0 s
t=20 s
t=40 s
t=60 s
t=90 s
steady state
T (C)
Axial Position (mm)
(c)
t=0 s
t=20 s
t=40 s
t=60 s
Steady state
T (C)
Axial Position (mm)

Fig. 8

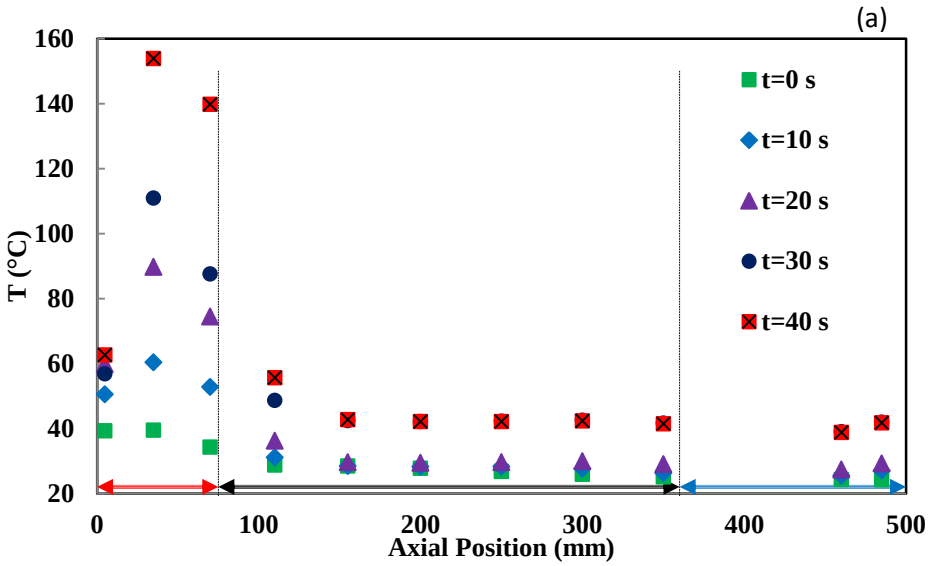
(a)
160
140
120
100
80
60
40
20
T (°C)
0
100
200
300
400
500
Axial Position (mm)
t=0 s
t=10 s
t=20 s
t=30 s
t=40 s

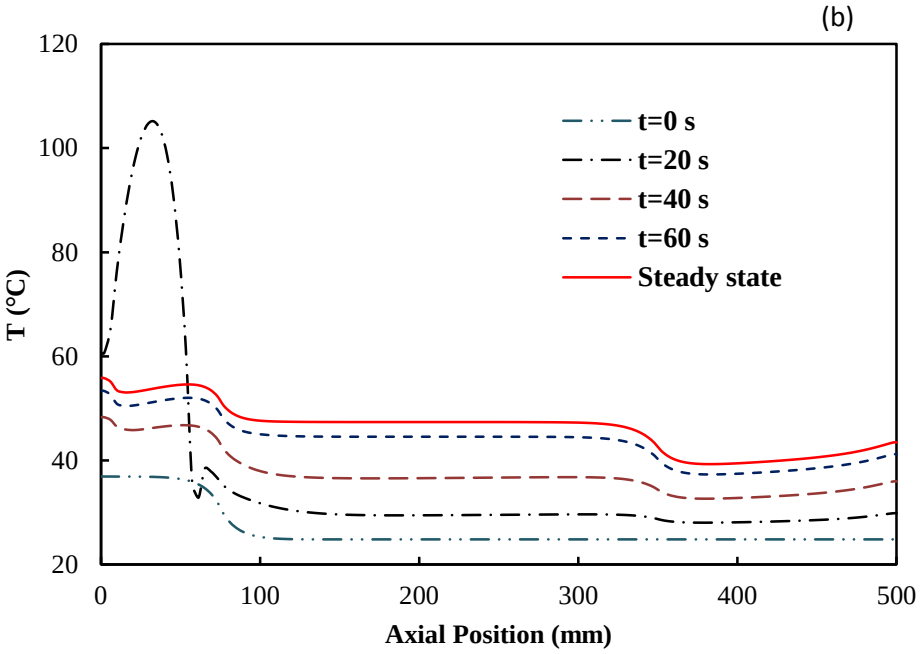
(b)
120
100
80
60
40
20
T (°C)
0
100
200
300
400
500
Axial Position (mm)
t=0 s
t=20 s
t=40 s
t=60 s
Steady state

Fig. 9

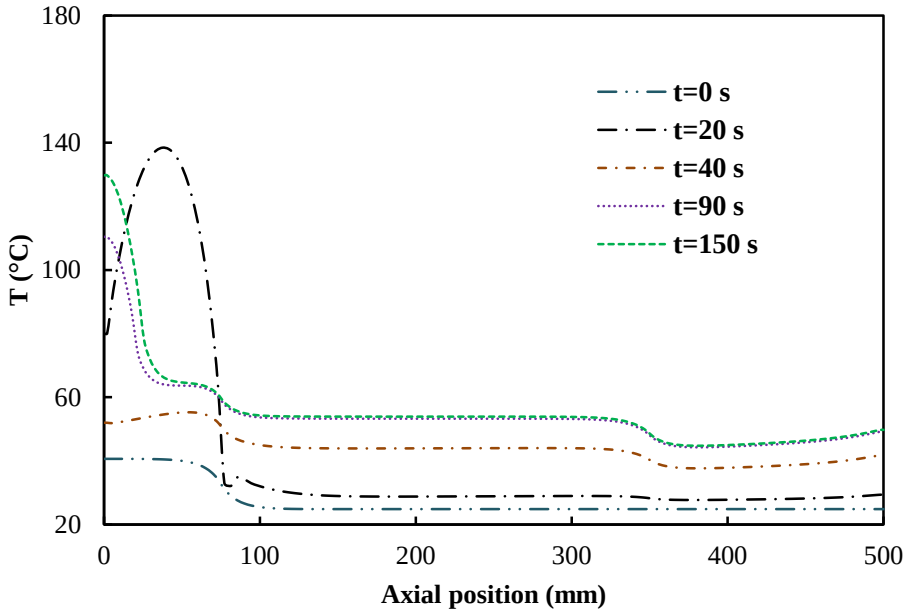
180
140
100
60
20
T (°C)
0
100
200
300
400
500
Axial position (mm)
t=0 s
t=20 s
t=40 s
t=90 s
t=150 s

Fig. 10

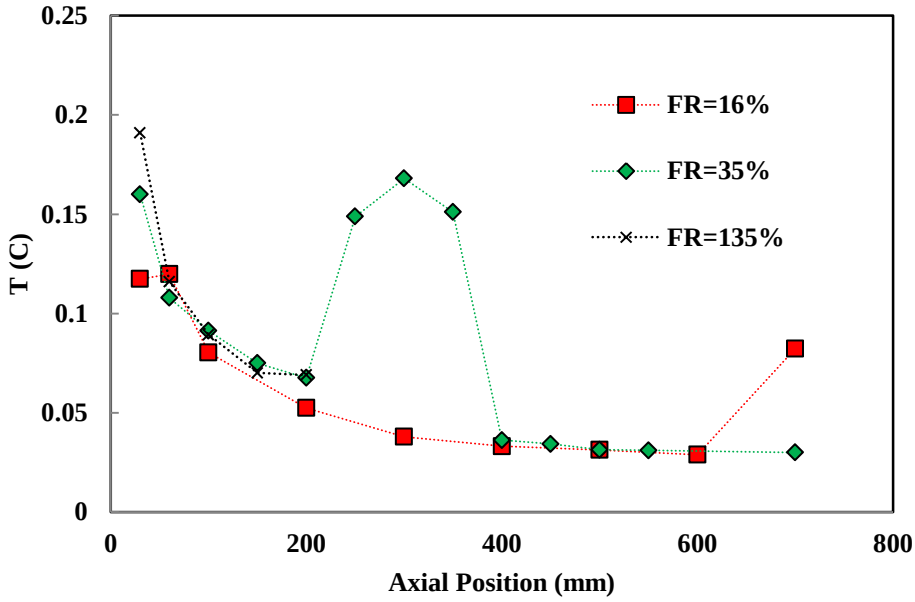
0.25
0.2
0.15
0.1
0.05
0
T (C)
0
200
400
600
800
Axial Position (mm)
FR=16%
FR=35%
FR=135%

Fig. 11

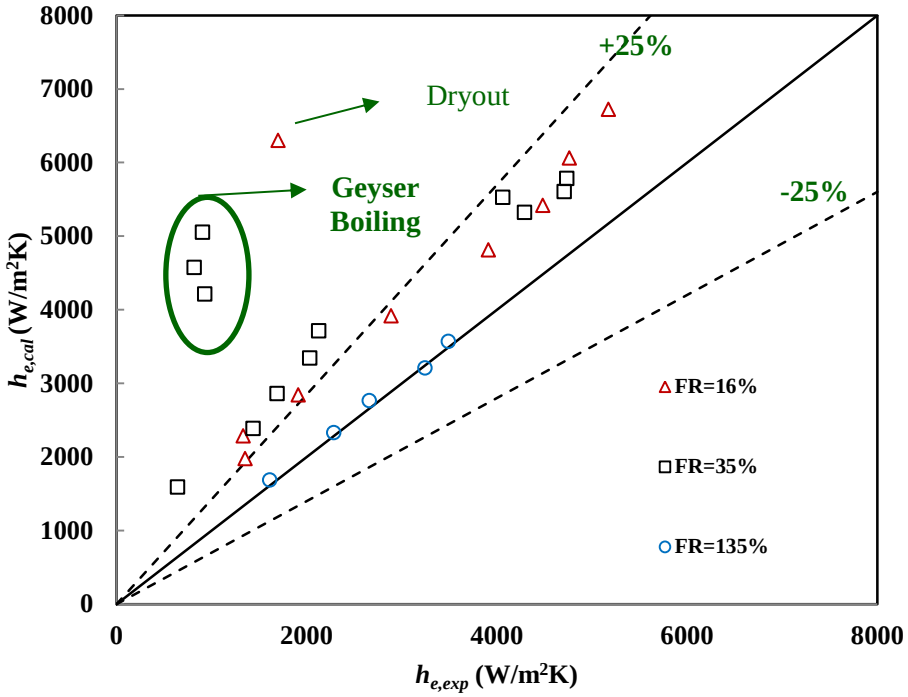
8000
7000
6000
5000
4000
3000
2000
1000
0
0
2000
4000
6000
8000
$h_{e,cal}$ (W/m^{2}K)
$h_{e,exp}$ (W/m^{2}K)
+25%
-25%
Dryout
Geyser
Boiling
FR=16%
FR=35%
FR=135%

Fig. 12.

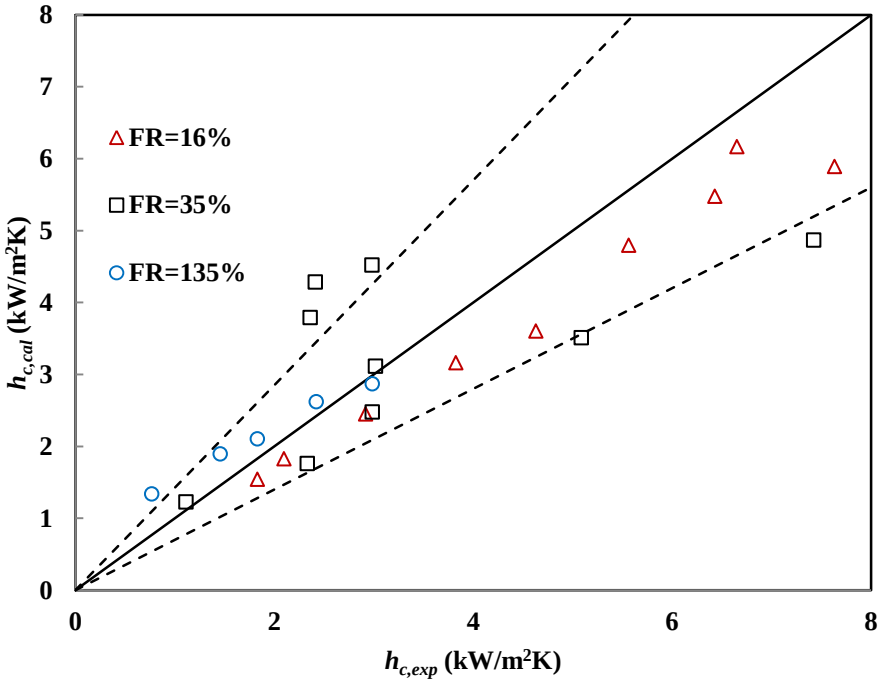
8
7
6
5
4
3
2
1
0
0
2
4
6
8
$h_{c,cal}$ (kW/m^{2}K)
$h_{c,exp}$ (kW/m^{2}K)
FR=16%
FR=35%
FR=135%

Fig.13

Tables

Table 1 Design summery of TPCT applied in experiments and numerical simulation
Table 2 Operating conditions of the TPCT

Table 1

Wall		**heat transfer fluid (liquid)**		**heat transfer fluid (vapour)**	
Wall Material	Copper	Working fluid	Water	Thermal conductivity, (W/mK)	0.028
Outer radius, (mm)	35	Thermal conductivity, W/mK)	0.67	Specific heat, (J/kgK)	2410
Thickness, (mm)	1	Density, (kg/m3)	925	viscosity (Pa s)	1.3×10^{-5}
Total length, (mm)	500	Latent heat, (kJ/kg)	2140	T_0 (C)	25
Evaporator length, (mm)	75				
Condenser length, (mm)	150	viscosity (Pa s)	2.2×10^{-4}	P_0 (Pa)	3.1×10^{3}
Thermal conductivity, (W/mK)	350				
Specific heat, (J/kgK)	380				
Density, (kg/m3)	8900				

Table 2

Parameters	
Cooling mass flow meter, (kg/s)	0.038
Inlet cooling temperature, (°C)	25±0.25
Input heat flux, (W)	30-700
Filling ratio (working fluid volume/evaporator volume), (%)	16, 35, 135